RSC Advances

ROYAL SOCIETY OF CHEMISTRY

www.rsc.org/advances

RSC Advance

RSCPublishing

ARTICLE

Visible-Light-Responsive t-Se Nanorods Photocatalysts: Synthesis, Properties, and Mechanism

Cite this: DOI: 10.1039/x0xx00000x

Ruofang Zhang,[a] Xike Tian,[a]* Longlong Ma,[a] Chao Yang,[a] Zhaoxin Zhou,[a]* Yanxin Wang,[b] Suhua Wang[c]

Received 00th January 2012,
Accepted 00th January 2012

DOI: 10.1039/x0xx00000x

www.rsc.org/

One-dimensional (1D) single-crystalline trigonal selenium nanorods (t-Se NRs) were prepared through a "solid-solution-solid" by dispersing the prepared amorphous α-Se spheres in ethanol. Single crystal structure of the t-Se NRs could be excited under visible light with the band gap of 1.56 eV. And the t-Se NRs were found for the first time to display noticeable photocatalytic activities under visible light. In addition, the rate of photodegradation of methyl orange (MO) in visible-Se NRs-H_2O_2 systems (1.7×10^{-1} min^{-1}) is about 17 times greater than that in visible-Se NRs-HCl system (1.0×10^{-2} min^{-1}) with equal pH. Furthermore, we proposed the photocatalysis mechanism of visible-Se NRs-H_2O_2 systems based on Electron Paramagnetic Resonance (EPR) characterization and studying the effect of different reactive species.

Introduction

Due to the wide application of visible-light-responsive photocatalysts in solar energy conversion, the search for visible-light-responsive photocatalyst has been an urgency endeavor worldwide. In addition to the overwhelming attention on compound photocatalysts, researchers have also begun to explore new efficient photocatalysts and then, their attention was now focused on the elemental semiconductors,[1] such as crystalline silicon (Si),[2,3] α-sulfur (S),[6] selenium (Se),[4] and red phosphorus (P).[5]

Among the elemental semiconductor photocatalysts, trigonal selenium is seen to be very crucial material, due to its good semiconducting behavior with an indirect band-gap value of near 1.8 eV as well as unique physical properties such as low melting point (about 490 K). Its other excellent attributes also include catalytic activity to hydration and oxidation reactions, anisotropy of the thermoconductivity, high photoconductivity, superconductivity, high piezoelectric, thermoelectric and nonlinear optical responses, etc.[7-9] Hence, the outlook of its applications is promising in many attractive fields, such as semiconductor solar cells, rectifiers, xerography, hoto cells, pigments, glasses industry, photographic exposure meter and as hard templates for the preparation of valuable semiconducting materials.[8,10-14]

There are several allotropic forms of selenium: three monoclinic forms α-, β-, and γ-selenium with Se_8 molecules, rhombohedral selenium with Se_6 molecules, trigonal selenium (t-Se) with Se_n molecules, and amorphous selenium. The t-Se is one of the most thermodynamically stable and the densest form that can act as a semiconductor with electrical conductivity values between 10^{-6} to 10^{-5} Ω^{-1} cm^{-1} at room temperature.[8,15,16] The structure of t-Se contains covalently bonded Se atoms which are arranged helically in infinite chains. The helical chains are trigonally bound together via van der waals force in the hexagonal lattice.[17] As a result, one-dimensional (1D) t-Se is expected to have a growth tendency along c-axis direction. There are several synthetic methods to germinate 1D Se nanostructures, for instance, by the sonochemical method,[18-21] carbothermal chemical vapor deposition (CTCVD),[23] chemical vapor deposition (CVD),[22] free template hydrothermal methods,[24-29] template-assisted methods, liquid-liquid interface technique, and biomolecule-assisted routes,[30-33] and so on. In the past decade, efforts have been made to prepare selenium nanostructures for the further development of selenium.

It has been recently reported that the elemental selenium prepared by the selenium compound reduction in liquid phase is usually the α-Se phase. However, many factors like temperature, light, and ultrasound can affect the conversion of α-Se to t-Se. So it still remains a challenge to efficiently convert α-Se to t-Se under ambient conditions. Saunders studied the phase change from the α-Se to t-Se or m-Se in different organic solvents a century ago.[34] Recently, a quantity of studies by Younan Xia showed that ultrasonic sound could significantly speed up the process of transforming the α-Se to t-Se.[35]

In this work, we developed a quick and easy method to prepare mass and super-long single-crystalline t-Se NRs at room temperature by transforming α-Se to t-Se by dispersing the prepared amorphous α-Se spheres in ethanol. And then, the photocatalytic degradation ability of MO by t-Se NRs in visible light region (λ>420 nm) was investigated. In the process of catalytic degradation, we found that

the addition of H_2O_2 in the system greatly increases the photocatalysis rate, and the photocatalysis rate also rises modestly along with the increasing the amount of H_2O_2.

Experimental

Chemicals

All chemicals were analytical grade and used without further purification.

Characterization

The crystallographic structure of the samples was explored by X-ray diffraction (XRD, Rigaku D/Max-RB (Cu Kα, λ = 1.5418 Å)). The morphology and dimensions of the products were investigated with field emission scanning electron microscope (FESEM) of Hitachio S-4800, transmission electron microscope (TEM) and selected area electron diffraction (SAED) of JEOL 2000 EX, High resolution TEM (HRTEM) and energy-dispersive spectrometry (EDS) of Czech FEI Company of Tecnai G220 S-TWIN. The optical properties of the product were researched with UV/Vis diffuse reflectance spectra (DRS) of PerkinElmer Lambda 35 UV/Vis spectrometer. UV-vis absorption spectra were obtained using a PerkinElmer Lambda 35 UV/Vis spectrometer at 25 ℃.

Synthesis of t-Se NRs

The synthesis of t-Se NRs was carried out by chemical reduction through a "solid-solution-solid" process. SeO_2 (0.001 M) and ascorbic acid (0.002 M) were first dissolved in 10 mL of deionized water, respectively. Then the ascorbic acid aqueous solution was added slowly to the H_2SeO_3 aqueous solution, accompanied by color change from colorless to orange and finally deep red. After the reaction completely, the suspension was centrifuged for 10 min, and the precipitate was then washed several times with distilled water. The precipitate was taken out to a small beaker containing 20 mL of ethanol and stirred for 1 h at room temperature. And the suspension changed from red to brown and finally into black by ageing 24 h. The black precipitate was collected and washed for several times with distilled water and absolute ethanol. Then the sample was dried in vacuum at 60 □ for 24 h.

Evaluation of photocatalytic performance

The photocatalytic activity of t-Se NRs was evaluated in terms of the degradation of methyl orange (MO) upon visible irradiation, as we call the visible-Se NRs system below. The photo-degradation of MO was compared between visible-Se NRs system and added different amount of H_2O_2, named visible-Se NRs-H_2O_2 system. The same light source Xe lamp (PLS-SXE 300) was used with 420 nm cutoff to get visible light. In each experiment, 50 mg of the photocatalysts was dispersed in 80 mL aqueous solution containing the given concentrations of MO. Prior to irradiation, the suspensions were magnetically stirred in dark for 60 min and exposed under the light irradiation. 5 mL of the suspension was then sampled and centrifuged to remove the solid photocatalysts every 20 min. The MO concentration variations were monitored with a UV-vis spectrophotometer from their characteristic absorption bands (generally 465 nm for MO).

Electron Paramagnetic Resonance (EPR) analysis

EPR experiments were carried out to research the hydroxyl radicals (·OH) generation capability of t-Se NRs. EPR spectra were recorded using a Bruker A300-10/12 EPR spectrometer at room temperature of two experimental systems under visible light radiation. The system named t-Se NRs system for the measurement was prepared by adding the spin-trapping reagent (5, 5-dimethyl-1-pyroline-N-oxide, expressed as DMPO, 0.1 M) to 5 mg/mL nanomaterial suspension. The suspension was then transferred to an EPR tube and then the tube was illuminated with greater than 420 nm visible light for 3 min. After the illumination, the EPR measurement was performed immediately. The another system called t-Se NRs-H_2O_2 system for the measurement was prepared by adding additional 0.5 M H_2O_2 into the system before visible light illuminated and the experimental procedure kept as the same as Se NRs system.

Results and discussion

Structural investigation

The XRD pattern of the product well matches with the typical powder XRD pattern of t-Se, as shown in Fig. 1a. All the reflection peaks can be indexed to be a trigonal phase of selenium (JCPDS card code 06-0362), whereas no any diffraction peaks attributing to the precursor SeO_2 or other impurities cannot be observed, indicating that the current process for production of pure t-Se was completely successful. What' more, all the observed peaks in the XRD (Fig. 1a) can be indexed onto the P3121 space group with the unit cell parameter a = 4.357Å, c = 4.963Å; α = β = 90°, γ = 120°, which are in consistent with both the standard (JCPDS card code No. 06-0362) and the published literature.[7, 19, 36-38]

Chemical analysis using energy-dispersive X-ray spectroscopy (EDS) shows the pure composition of Se in Fig. 1b, Cu and C signal is from the holey carbon film grids. The SAED (*inset* in Fig. 1c) is taken from a single t-Se NRs, which displays the crystalline structure of t-Se. The bright diffraction spots may be indexed as (001), (100) and (101) of Se (JCPDS card No. 06-0362), respectively. The SAED results indicate that the growth of the nanorods is along the [001] direction, which is in consistent with the literature.[19-21,56] Therefore, it can be proposed the reduction of H_2SeO_3 by ascorbic acid would spontaneously occur to initially form amorphous elemental α-Se at room temperature, and then followed by the anisotropic crystal growth of t-Se in ethanol. The crystal seeds subsequently grew along a preferred direction to generate relatively uniform dimension nanorods.

A high-resolution TEM (HRTEM) image obtained from the t-Se NRs edge is displayed in Fig. 1d, which gives rise to a d-spacing of about 0.19 nm corresponding to the (200) planes of trigonal Se. It is shown that the nanorods are grown anisotropically. This image also reveals that the t-Se NRs is single crystalline. Moreover, the corresponding fast Fourier transformation (FFT) pattern (*inset* in Figure 1d) can emphasize that t-Se NRs is single-crystal structure.

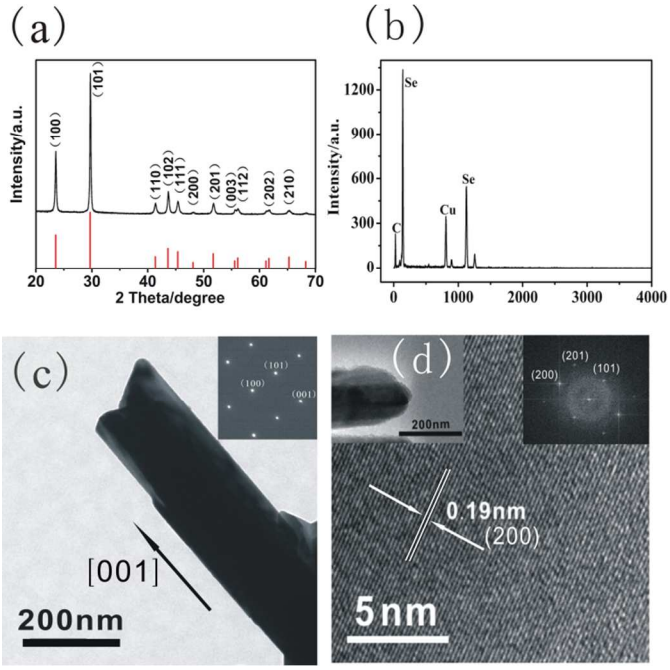

Fig. 1 (a) XRD pattern of t-Se NRs. (b) EDS of t-Se NRs the pure composition. (c) TEM image and SAED of a t-Se NRs (The corresponding electron diffraction pattern was obtained from the same Se nanorod, shown in the inset). (d) HRTEM image obtained from the edge of the individual t-Se NRs sample in the top-left inset. The top-right inset in (d) is the fast Fourier transform (FFT) of the HRTEM image.

Optical properties of t-Se NRs.

Two factors, the adsorption of target contaminant molecules and the intrinsic electronic properties of photocatalysts, containing the band-edge potential, the band gap, and charge-carrier mobility, are crucial in the photocatalytic process.[39] The UV-vis diffuse reflectance spectrum (DRS) of t-Se NRs is presented in Fig. 2a. It can be seen that the absorption stopping edge of Se NRs exhibits a noticeable result in the long-wavelength region, and the broadened absorption in the visible light region of t-Se NRs could cause an enhanced visible light photocatalytic activity. The band gap energies (hν) of samples are estimated from DRS, as shown in Fig. 2b. The plot of the Kubelka-Munk functions (F(R)) against the photon energy (hν) exhibits that the hν estimated from the intercept of the tangent to the plot is 1.56 eV.

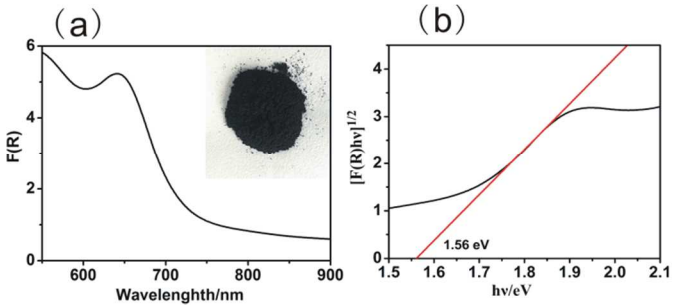

Fig. 2 (a) Kubelka-Munk function (F(R)) of t-Se NRs, the inset in (a) is a photograph of the t-Se crystal powder (b) Plot of the extraction of a root of the F(R) versus the photon energy (hν).

Growth mechanism

In order to examine the formation process of the t-Se NRs, the morphological evolution with various ageing time in ethanol was investigated. As displayed in Fig. 3a, the red spherical Se particles of about 200 nm in size first formed at the early stage of reaction. Some particles then grew adjacently to each other to form worm-like particle aggregations. The particle aggregations and the individual particles subsequently grew out to form branched structures to evolve the 1-D architecture (Fig. 3b, c). Continued longitudinal growth in these quasi-1-D structures finally led to the formation of nanorods with uniform dimensions, as in Fig. 3d. These t-Se NRs had a typical diameter of about 100~200 nm and length from several microns to dozens of microns. On the basis of the above results, a growth mechanism for the present Se NRs was proposed and illustrated in Fig. 3e. The initial suspension, containing a mixture of α-Se colloids and t-Se nanocrystallites, was aged in ethanol at room temperature. Then the α-Se colloids could slowly dissolve into the solution phase and form worm-like aggregations because of its higher free energy compared to t-Se. Subsequently, the worm-like aggregations could be deposited on the surfaces of t-Se seeds and slowly grew, as single crystalline t-Se NRs. In this solid-solution-solid transformation,[40] the 1D morphology of the final product was determined by the highly anisotropic characteristics of the building blocks-that is, the linearity of infinite, helical chains of Se atoms contained in the trigonal phase. Abdelouas et al.[41] reported a synthetic method with cytochrome C as the reducing agent for Se nanowires, which were chain-like aggregates of nanoparticles of three monoclinic forms of Se rather than single crystalline. And now, uniform t-Se NRs as we have obtained here.

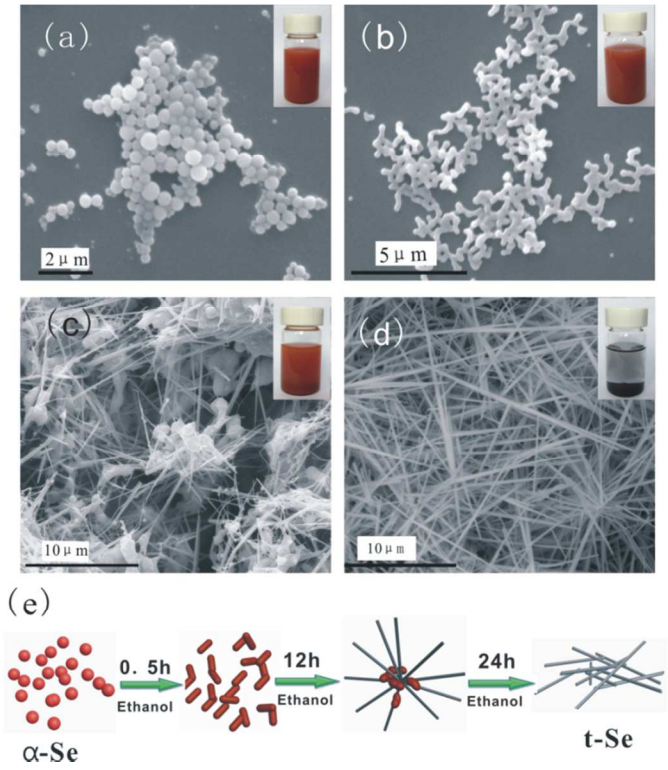

Fig. 3 FESEM images of Se samples obtained at various ageing times in ethanol: (a) 5 min, (b) 0.5 h, (c) 12 h, (d) 24 h, the insert in (a) (b) (c) and (d) show photographs of suspension liquids. Schematic illustration of a growth mechanism for the formation of t-Se NRs via a solid-solution-solid pathway in (e): Reduction of selenious acid with ascorbic acid in an aqueous solution produces mono-dispersed spherical colloids of α-Se which are ~200 nm in diameter, then these α-Se aggregate after ageing 0.5 h in ethanol, t-Se NRs grow from those aggregate after ageing 12 h due to Rayleigh instability, finally, continued longitudinal growth in these 1-D structures led to the formation of naonorods with uniform dimensions ageing 24 h.

Photocatalytic activities

Effect of H_2O_2 on the photodegradation of MO with t-Se NRs

Fig. 4a shows that the dye MO (the initial concentration of 20 mg/L) cannot be directly photodegraded in the presence of only H_2O_2 by visible light irradiation for 80 min. This is because of that the energy of visible light irradiation is too low to directly photolyze H_2O_2 to produce ·OH. However, when the photodegradation experiments of MO were conducted in the system of t-Se NRs, its efficiency greatly increased, indicating the high yield of active species production by t-Se NRs (Fig. 4a). A H_2O_2 molecule cannot be split directly to generate ·OH to degrade pollutants under the irradiation of visible light, therefore the photodecomposition of H_2O_2 in the presence of t-Se NRs under visible light might be due to the catalysis by t-Se NRs. In the process of t-Se NRs photocatalysis, the photocatalytic rate increased moderately with increase of the amount of H_2O_2. The photodegradation of MO in the visible-Se NRs-H_2O_2 systems fit a pseudo-first-order kinetics model, as described in Eq.1

$$\ln(\frac{C_0}{C}) = Kt \qquad \text{Eq.1}$$

where C_0 and C are the concentrations of MO (mg/L) at the initial time and at the reaction time t (min), respectively; K is the pseudo-first-order reaction rate constant (min^{-1}).

The amount of H_2O_2 (30%) was 0, 1 mL, 2 mL, 5 mL, corresponding to the photocatalytic rate constant of 2.0×10^{-2} min^{-1}, 0.93×10^{-1} min^{-1}, 1.16×10^{-1} min^{-1}, 1.7×10^{-1} min^{-1}, respectively, as Table 1 showed. Fig. 4b showed the photographs of different system after irradiation different time, respectively. The solutions in A and B keep the initial colour after irradiation 80 min, which proved that H_2O_2 cannot be photolyzed to produce ·OH and degrade MO under visible light. The solutions in C and D show that the colour of the solution faded away gradually with radiation longer, which indicates that t-Se NRs could efficiently photodegradate MO quickly under the visible light. The solution in E displays that the colour of the solution faded completely after irradiation 20 min, which imply that H_2O_2 could promote the t-Se NRs photocatalytic rate greatly under visible light.

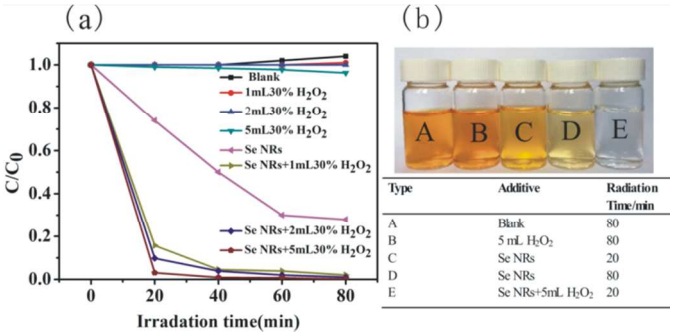

Type	Additive	Radiation Time/min
A	Blank	80
B	5 mL H_2O_2	80
C	Se NRs	20
D	Se NRs	80
E	Se NRs+5mL H_2O_2	20

Fig. 4 (a) The graph of photocatalytic degradation MO. (b) The photographs of different systems after irradiation different time, respectively. The table under the photographs shows the information of different systems in detail.

Table 1 Photocatalytic degradation removal of MO and using 0.625 g/L of t-Se NRs as a catalyst. The reaction was carried out in visible light, room temperature conditions; the 30% H_2O_2 addition was 1, 2, 5 mL and the initial concentration of MO was 20 mg/L.

Additive	Duration Time/min	Degradation (%)	Kinetic constant K(min^{-1})
Blank	80	0	0
5mL H_2O_2	80	0	0
Se NRs	60	~70	2×10^{-2}
Se NRs+1mLH_2O_2	20	~85	0.93×10^{-1}
Se NRs+2mLH_2O_2	20	~90	1.16×10^{-1}
Se NRs+5mLH_2O_2	20	~100	1.7×10^{-1}

In order to exclude the pH effects of the addition of H_2O_2 on t-Se NRs photodegradation of MO, we adjusted the pH of MO solution before photocatalysis with H_2O_2 and HCl, to make both of them be 5.4, which named visible-Se NRs-H_2O_2 system and visible-Se NRs-HCl system, respectively. From Fig. 5, we can see that the rate constant (1.7×10^{-1} min^{-1}) of photocatalytic in H_2O_2 system is about 17 times greater than that in HCl system (1.0×10^{-2} min^{-1}) with equal pH. Therefore, we proved that it was the presence of H_2O_2 rather than the changed pH that promoted the photocatalysis and the introduction of H_2O_2 greatly accelerated the catalytic rate.

The spent t-Se NRs is characterized after photocatalytic in the visible-Se NRs-H_2O_2 systems shown in Fig. S1. Fig. S1a shows the XRD pattern of the spent t-Se NRs. All the peaks can be readily indexed to crystalline trigonal selenium (t-Se) (JCPDS 06-0362), which implied the photocatalytic process in the visible-Se NRs-H_2O_2 systems has no effect on crystal structure of t-Se. Fig.S1b shows that the morphology of the spent t-Se NRs remains 1D nanorods structure. The result of XRD and SEM test indicates that the presence of H_2O_2 in the visible-Se NRs-H_2O_2 systems will not affect the crystal structure and morphology of t-Se NRs.

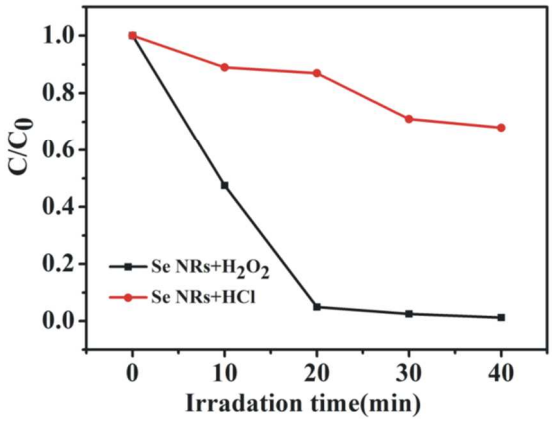

Fig. 5 Comparing the photodegradation of MO with different systems under the same pH.

EPR study of photogenerated hydroxyl radicals (·OH)

The EPR is an effective technical method in identification of active radicals. Hydroxyl radicals account for the primary role for most of the photocatalysis processes in aqueous solutions, so the EPR and spin-traping technique were used to investigate the production of hydroxyl radical. The EPR spectra obtained after visible light irradiation of DMPO and t-Se NRs alone or t-Se NRs + H_2O_2 were identical according to peak locations and the characteristic of 1:2:2:1 relative peak magnitudes in association with trapped ·OH radicals in the form of DMPO-OH,[42-47] as shown in Fig. 6. The presence of H_2O_2 in the reaction suspension had little effect on peak locations, but enhanced the peak magnitudes substantially. The result shows that the addition of H_2O_2 to the system is able to increase the concentration of DMPO-OH, demonstrating higher rates of ·OH radicals generation after addition of H_2O_2.

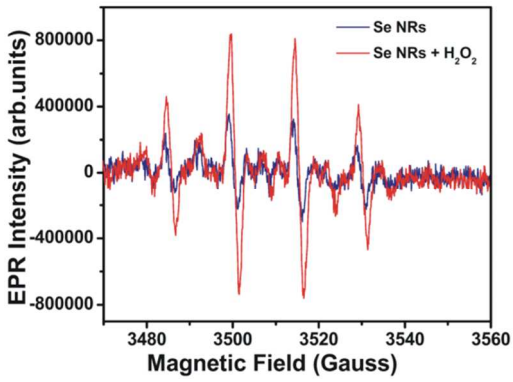

Fig. 6 The EPR spectra obtained on visible light irradiation of DMPO and Se NRs alone or Se NRs + H_2O_2.

The mechanism of H_2O_2 promoting photocatalytic

In order to explain the mechanism of H_2O_2 promoting t-Se NRs visible light catalytic, we should research the photodegradation mechanism of t-Se NRs under visible light, by control experiments involving in the effect of photodegradation on scavenger agents of isopropyl, triethanolamine, and p-benzoquinone, respectively. As shown in Fig. 7a, when 10 mM isopropyl, triethanolamine or p-benzoquinone was added in the visible-Se NRs systems, respectively, the photodegradation rate constant was slowed down. Isopropyl groups would effectively scavenge ·OH, triethanolamine would effectively scavenge h^+, and p-benzoquinone would effectively scavenge $\cdot O_2^-$, therefore, it was deduced that ·OH, $\cdot O_2^-$ and h^+ were the active species for the degradation of MO in the visible-Se NRs systems. Among the active species, ·OH was the mainly active species for the degradation of MO in visible-Se NRs systems.

When adding 5 mL H_2O_2 (30%) into the visible-Se NRs system, the rate of photocatalytic degradation of MO increased rapidly. But when isopropyl was added in the visible-Se NRs-H_2O_2 systems, isopropyl would effectively scavenge ·OH, with a high reaction rate constant.[55] Thus, the presence of isopropyl significantly suppressed the degradation of MO, as shown in Fig. 7b. While p-benzoquinone was added in the visible-Se NRs-H_2O_2 systems, p-benzoquinone suppressed a little the degradation of MO. The reason was that one part of electrons in conduction band of t-Se NRs were captured by oxygen molecules to generate $\cdot O_2^-$ radicals, and then react with H^+ and triggered a series of reaction to generate ·OH quickly in acid solution. Therefore, it was deduced that ·OH was the mainly active species for the degradation of MO in the visible-Se NRs-H_2O_2 systems. In the visible-Se NRs-H_2O_2 systems, ·OH could be generated from the reduction of H_2O_2 by conduction-band electrons (e_{CB}).

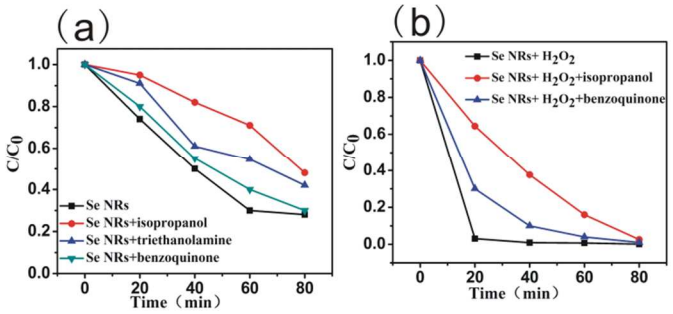

Fig. 7 Degradation curve of MO in various systems (a) visible-Se NRs systems, (b) visible-Se NRs-H_2O_2 systems.

When the energy of an incident light surpasses the band gap energy of the photocatalyst during the process of photocatalysis, electrons in the valence band will be activated into the conduction band (e_{CB}), and leaving holes in the valence band (h_{VB}^+). At pH=5.4, the bottom of the conduction band E_{CB} has been deduced as -0.5 V (*vs*. NHE) for t-Se.[51,52] For t-Se, the E_{CB} is more negative than the H_2O_2/·OH redox potential, which is 0.87 V (*vs*. NHE). Thus, in the presence of Se NRs under visible light, H_2O_2 can be reduced to ·OH when receiving e_{CB} (Eq.2).[53-55] The result of visible light catalytic degradation of MO in visible-Se NRs-H_2O_2 systems indicates higher rates of ·OH radical generation, which consistent with the result of EPR study.

$$H_2O_2 + e_{CB} \rightarrow \cdot OH + OH^- \qquad \text{Eq. 2}$$

As shown in Eq. 2, H_2O_2 can be reduced by e_{CB} to yield the very active ·OH, which may result in the degradation of MO. Compared the decompositions of MO in the visible-Se NRs-H_2O_2 systems and the visible-Se NRs-HCl systems, it was shown that, the degradations of MO in visible-SeNRs-H_2O_2 systems are much faster than in visible-Se NRs-HCl systems. This indicated that H_2O_2 could be decomposed to generate the active species of ·OH, which consistent with the result of the photocatalysis of isopropyl scavenger agents. As discussed above, H_2O_2 could be reduced to ·OH by the photogenerated electrons, since the redox potential of H_2O_2/·OH is 0.87 V (*vs*. NHE), H_2O_2 can be reduced to ·OH, which is consistent with the literature.[55]

When t-Se NRs-H_2O_2 system is illuminated by visible light irradiation, the generation route of ·OH in visible-SeNRs-H_2O_2 system has displayed in Scheme 1, the photons excite the valence band electrons across the band gap into the conduction band and one part of electrons in conduction band react with oxygen molecules and hydrogen ion in surface of catalyst to generate ·OH radicals.[48,49] The another part of electrons can be captured by H_2O_2 molecules and generate ·OH radicals, which consistent with the result of above. What's more, h^+ in valence band also can react with H_2O molecules to generate ·OH radicals.[57] The azo bond which is abundant in electrons in MO, is mainly attacked by ·OH radicals. This results in the cleavage of the azo bond in MO and causes decolorization of the dye solution.[50] Schematic illustration of the photocatalysis mechanism of visible-Se NRs-HCl system and visible-Se NRs-H_2O_2 system is shown in Fig. S2. It shows the visible light catalytic mechanism of t-Se NRs and the promoting photocatalytic mechanism of additional H_2O_2. This result reveals that the prepared t-Se NRs could be promisingly utilized in the long-term course of photocatalysis.

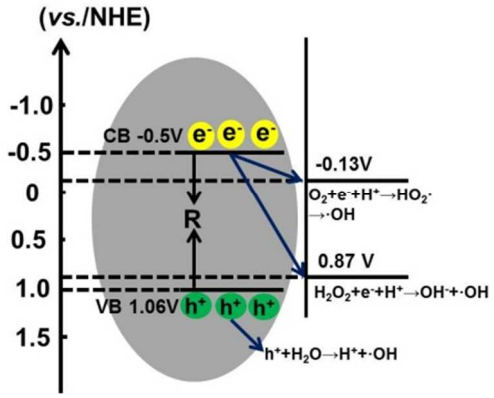

Scheme 1 The production process of ·OH in visible-SeNRs-H_2O_2 system.

Conclusions

In summary, we have successfully developed a facile chemical reduction approach for the preparation of single-crystalline t-Se NRs. t-Se NRs are found to be of noticeable photocatalytic activities under visible light for the first time. The results of photocatalytic degradation of MO show t-Se NRs process the good catalytic property in visible light, which is due to their single crystal structure that can be excited under visible light with the band gap of 1.56 eV. In addition, a higher rates of ·OH radical generated in visible-Se NRs-H_2O_2 system are proved according to studying the effect of different reactive species and EPR characterization. Therefore, H_2O_2 can promote the t-Se NRs photocatalytic efficiency under visible light. The rate constant of photodegradation MO in visible-Se NRs-H_2O_2 systems (1.7×10^{-1} min^{-1}) is about 17 times greater than that in visible-Se NRs-HCl system (1.0×10^{-2} min^{-1}) with equal pH. There are three ·OH production approaches in visible-Se NRs-H_2O_2 system. When in the presence of hydrogen ions, e_{CB} can be captured by the oxygen molecules and H_2O_2 in surface of catalyst to generate ·OH radicals, respectively. In addition, h^+ in valence band also react with H_2O molecules to generate ·OH radicals. The mechanism of H_2O_2 promoting photocatalytic is that H_2O_2 could be reduced by a part of e_{CB} coming from t-Se NRs to ·OH. This study could offer a feasible industrial route to design high-performance visible light photocatalyst system.

Acknowledgments

The Authors would like to acknowledge financial supports from the National Basic Research Program of China (973 Program, Grant No. 2011CB933700) of the Ministry of Science and Technology of China, the National Natural Science Foundation of China (Grant No. 51371162 & 51344007), the Fundamental Research Funds for the Central Universities, and China Scholarship Council. Valuable suggestions of Prof. Abraham Clearfield at the Department of Chemistry Texas A & M University are also greatly acknowledged.

Notes and references

[a] Faculty of Material Science and Chemistry, China University of Geosciences, Wuhan 430074, P R China
[b] School of Environmental Studies, China University of Geosciences, Wuhan 430074, P R China
[c] Department of Chemistry, University of Science & Technology of China, Hefei, Anhui 230026, China
[*]Corresponding author: Xike Tian, Zhaoxin Zhou

Address: Faculty of Material Science and Chemistry, China University of Geosciences, No. 388 Lumo Road, Wuhan 430074, P R China
Tel.: +86 27 67884574; Fax: +86 27 67884574;

E-mail address: xktian@cug.edu.cn (Xike Tian),

zhaoxinzhou@cug.edu.cn (Zhaoxin Zhou)

1. G. Liu, P. Niu, H. M. Cheng, *ChemPhysChem.* 2013 **14** (5), 885-892.
2. Z. H. Kang, Y. Liu, C. H. A. Tsang., D. D. D. Ma, X. Fan, N. B. Wong, S. T. Lee, *Adv. Mater.* 2009, **21**, 661-664.
3. Z. H. Kang, C. H. A. Tsang, N. B. Wong, Z. D. Zhang, S. T. Lee, *J. Am. Chem. Soc.* 2007, **129**, 12090-12091.
4. Y. D. Chiou, Y. J. Hsu, *Appl. Catal. B* 2011, **105**, 211-219.
5. F. Wang, W. K. H. Ng, J. C. Yu, H. J. Zhu, C. H. Li, L. Zhang, Z. F. Liu, Q. Li, *Appl. Catal. B* 2012, 111-112.
6. G. Liu, P. Niu, L. C. Yin, H. M. Cheng, *J. Am. Chem. Soc.* 2012, **134**, 9070-9073.
7. B. Gates, Y. Wu, B. Cattle, Y. N. Xia, *Adv. Funct. Mater.* 2002, **12**, 219-227.
8. R. A. Zingaro, W. C. Cooper, Eds. Selenium; Litton Educational Publishing: New York 1974; **25**, 174-217.
9. L. I. Berger, *Semiconductor Materials*; CRC Press: Boca Raton, FL, 1997, **86**.
10. S. Y. Zhang, C. X. Fang, Y. P. Tian, K. R. Zhu, B. K. Jin, Y. H. Shen, J. X. Yang, *Cryst. Growth Des.* 2006, **6**, 2809.
11. X. C. Jiang, B. Mayer, T. Herricks, Y. N. Xia, *Adv. Mater.* 2003, **15**, 1740.
12. B. Gates, Y. Y. Wu, Y. D. Yin, P. D. Yang, Y. N. Xia, *J. Am. Chem. Soc.* 2001, **123**, 11500.
13. H.T. Li, P.J. Regensburger, *J. Appl. Phys.* 1963, **34**, 1730-1734.
14. J.A. Johnson, M.L. Saboungi, P. Thiyagarajan, R. Csencsits, D. Meisel, *J. Phys.Chem. B* , 1999, **103**, 59-63.
15. N. N. Greenwood, A. Earnshaw, *Chemistry of the Elements*, Pergamon Press: Oxford 1984, 888.
16. D. C. Yao, J. H. Yung, *Applied Catalysis B: Environmental.* 2011, **105**, 211-219.
17. A. V. Hippel , *J. Chem. Phys.* 1948, **16**, 372.
18. B. Mayers, Y. Xia, *Adv.Mater.* 2002, **14**, 1749.
19. X. Li, Y. Li, S. Li, W. Zhou, H. Chu, W. Chen, I. L. Li, Z. Tang, *Cryst. Growth Des.* 2005, **5**, 911.
20. L. Ren, H.Z. Zhang, P.H. Tan, Y.F. Chen, Z.S. Zhang, Y.Q. Chang, J. Xu, F.H. Yang, D.P. Yu, *J. Phys. Chem. B* 2004, **108**, 4627-4630.
21. L.B. Luo, X.B. Yang, F.X. Liang, J.S. Jie, Q. Li, Z.F. Zhu, C.Y. Wu, Y.Q. Yu, W. Li, *Cryst.Eng.Comm.*,2012, **14**, 1942-1947.
22. X. B. Cao, Y. Xie, S. Zhang, F. Li, *Adv. Mater.* 2004, **16**, 649.
23. H. Zhang, M. Zuo, S. Tan, G. Li, S. Zhang, J. Hou, *J. Phys. Chem.B* 2005, **109**, 10653.
24. G. Xi, K. Xiong, Q. Zhang, R. Zhang, H. Zhang, Y. Qian, *Cryst.Growth Des.* 2006, **6**, 577.
25. C. An, K. Tang, X. Liu, Y. Quian, , *Eur. J. Inorg. Chem.* 2003, 3250.
26. Y. Ma, L. Qi, , J. Ma, H. Cheng, *Adv. Mater.* 2004, **16**, 1023.
27. M. Chen, L. Gao, *Chem. Phys. Lett.* 2006, **417**, 132.
28. Q. Xie, , J. Liu, J. Liang, W. Yu, Y. Quian, *J. Nanosci. Nanotech* 2006, **6**, 857.
29. Q. Xie, Z. Dai, W. Huang, W. Zhang, D. Ma, X. Hu, Y. Qian, *Cryst. Growth Des.* 2006, **6**, 1514.
30. N. Sudip, G. Sujit Kumar, Sudipa Panigahi,Thomas Thundat, Tarasankar Pal, *Langmuir* 2004, **20**, 7880-7883.
31. K. Mondal, P. Roy, K. S. Suneel, *Cryst. Growth Des.* 2008, **8**, 1580-1584.
32. Z.X. Chen, Y.H. Shen, A.J. Xie, J.M. Zhu, Z.F. Wu, H.Z. Huang, *Cryst. Growth Des.* 2009, **9,** 1327-1333.
33. Z.Y. Tang, Y. Wang, K. Sun, A. K. Nicholas, *Adv. Mater.* 2005, **17**, 358-363.
34. A. P. Saunders, *J. Phys. Chem.*, 1900, **4**, 423-513.
35. B. Gates, B. Mayers, B. Cattle, Y. N. Xia. *Adv. Funct. Mater.* 2002, **12**(3): 219
36. H. Zhang, D.R. Yang, Y.J. Ji, X.G. Ma, J. Xu, D.L. Que, *J. Phys. Chem. B* ,2004**, 108**, 1179-1182.
37. X.Y. Liu, M.S. Mo, J.H. Zeng, Y.T. Qian, *J. Cryst. Growth,* 2003, **259**, 144-148.
38. L. Liu, Q. Peng, Y. Li. *Nano Research*, 2008, **1**(5): 403-411.
39. X. M. Tu, S. L. Luo, G. X. Chen, J.H. Li, *Chem. Eur.J.* 2012, **18**, 14359-14366.
40. H. F.Yan, Y. J. Xing, Q. L. Hang, D. P. Yu, Y. P. Wang, J. Xu, Z. H. Xi, S. Q. Feng, *Chem. Phys. Lett*. 2000, 323-324.
41. A. Abdelouas, W. L. Gong, W. Lutze, J. Shelnutt, A. Franco, R. Moura, I., *Chem. Mater*. 2000, **12**, 1510.
42. T. Uchino, H. Tokunaga, M. Ando, H. Utsumi, *Toxicol.* 2002, **16**, 629-635.
43. V. Krishna, D. Yanes, W. Imaram, et al., *Appl. Catal. B: Environ.*, 2008, **79**(4): 376-381.
44. M. Y. Guo, A. M. C. Ng, F. Liu, et al., *Appl. Catal. B: Environ.*, 2011, **107**(1): 150-157.
45. T. Wu, T. Lin, J. Zhao, et al., *Environ. Sci. & Tech.*, 1999, **33**(9): 1379-1387.
46. M. D. Hernández-Alonso, A. B. Hungría, A. Martínez-Arias, et al., *Appl. Catal. B: Environ.*, 2004, **50**(3): 167-175.
47. J. M. Coronado, A. Javier Maira, A. Martínez-Arias, et al. *Journal of Photochemistry and Photobiology A: Chemistry*, 2002, **150**(1): 213-221.
48. J.C. Crittenden, Y. Zhang, D.W. Hand, D.L. Perram, E.G. Marchand, *Water Environ. Res.*, 1996, **68**, 270-278
49. W. Kangwansupamonkon, W. Jitbunpot, S. Kiatkamjornwong, *Polym. Degrad. Stab.* 2010, **95**, 1894-1902
50. A. O. Soon, M. M. Ohm, N. H. Li, S. W. Yee, *Environ. Sci. Pollut. Res.* 2013, **20**, 3405-3413
51. S. J. Fonash, 1981 Solar Cell Device Physics (New York: Harcourt Brace Jovanovich)
52. K. Tennakone, G. R. R. A. Kumara, I. R. M. Kottegoda, V. P. S. Perera , G. M. L. P. Aponsu, *J. Phys. D: Appl. Phys.* **31** (1998) 2326-2330.
53. P. Wardman, *J. Phys. Chem. Ref.* 1989, **18**.
54. T. Hirakawa, Y. Nosaka, , *Langmuir*, 2002**, 18**(8), 3247-3254.

55. Y. X. Du, L. Zhao, Y. Y. Zhang, *J. Hazard. Mater.* 2014, **267**, 55-61.
56. A. M. Qin, Z. Li, R. S. Yang, Y. D. Gu, *Solid State Communications* 2008, **148**, 145-147.
57. H. M. Yang, K. Zhan, R. Shi, *Journal of Alloys and Compounds* 2006, **413**, 302-306.